International Journal of Solids and Structures 108 (2017) 24–39

Contents lists available at ScienceDirect

International Journal of Solids and Structures

journal homepage: www.elsevier.com/locate/ijsolstr

Crease-free biaxial packaging of thick membranes with slipping folds

Manan Arya, Nicolas Lee[1], Sergio Pellegrino*

Graduate Aerospace Laboratories, California Institute of Technology, 1200 E. California Blvd., Pasadena CA 91125, USA

ARTICLE INFO

Article history:
Received 20 February 2016
Revised 26 July 2016
Available online 28 September 2016

Keywords:
Origami
Thick membranes
Deployable structures
Packaging

ABSTRACT

This paper presents a novel scheme to biaxially package and deploy flat membranes, in which the thickness of the membrane is accounted for through the novel concept of slipping folds. The membrane is divided into parallel strips connected by slipping folds, and specially chosen wrapping profiles that require zero slip along the edges of the membrane are identified. This packaging scheme avoids the kinematic incompatibilities that in other schemes result in local buckles and wrinkles that increase the deployment force and permanently deform the membrane. The paper also presents a scheme to apply uniform uniaxial prestress to the deployed membrane, as well as a two-stage deployment scheme. Packaging efficiencies of up to 83% have been demonstrated for meter-scale models, although for large membranes the packaging efficiency approaches 100%.

1. Introduction

Membranes are widely used in large-area space structures, including photovoltaic arrays, solar sails, drag sails, reflectors, transmissive optics, thermal shields, etc. These applications require tight packaging of the membranes for launch into orbit, followed by in-orbit deployment. This need for packaging and deployment poses three fundamental challenges: first, making efficient use of the stowage volume, leaving minimal voids; second, avoiding permanent deformation of the membrane material, i.e. remaining within the elastic limit; and, third, being able to deploy with small and predictable edge forces, to lower the requirements on the edge structure that will carry out the deployment (Arya, 2016).

The first of these challenges is well-known and has been addressed extensively in the literature, but the search for solutions to all three challenges combined, for the case of biaxial folding, is a problem still wide open.

This paper presents a novel scheme to biaxially package and deploy flat membranes. This packaging scheme accounts for the thickness of the membrane through the novel concept of slipping folds, which avoid the kinematic incompatibilities that in other schemes lead to the formation of buckles and wrinkles. These effects are responsible for decreased packaging efficiency, plastic deformation and non-smooth deployment.

The paper begins with a survey of the state of the art on the packaging of membrane structures, in Section 2. Section 3 presents the proposed packaging concept which, is called slip-wrapping, for the specific case of a square membrane. Section 4 shows that uniform, uniaxial prestress can be applied to rhombus-shaped membranes with curved edges, with slits that allow slip-wrapping. Section 5 presents a deployment scheme for slip-wrapped membranes. To validate the proposed packaging, deployment and prestressing schemes, experiments were carried out in the laboratory, using a simple apparatus that is described in Section 6. The test results are presented in Section 7, and Section 8 concludes the paper.

2. Background

Membrane packaging solutions can be divided into two broad categories, those providing compaction in one dimension, and those providing biaxial compaction. Folding is the most commonly used deformation mechanism. It can be accomplished either by creasing, i.e. by imposing a localized bending deformation of the membrane, or by incorporating mechanical hinges that allow rigid-body rotation of one part of the membrane with respect to another. Tight creasing results in plastic deformation, and a plastically creased membrane cannot be pulled flat using in-plane tension (Murphey, 2000; Papa and Pellegrino, 2008). Mechanical hinges, on the other hand, may be unfolded using in-plane tension alone, though they add mass and complexity to the structure.

* Corresponding author.
E-mail addresses: marya@caltech.edu (M. Arya), nnlee@stanford.edu (N. Lee), sergiop@caltech.edu (S. Pellegrino).
[1] Current address: Department of Aeronautics and Astronautics, Stanford University, 496 Lomita Mall, Stanford, CA 94305, USA

http://dx.doi.org/10.1016/j.ijsolstr.2016.08.013
0020-7683/

Nomenclature

A	Area
c	Pitch of involute curve
D	Bending stiffness
D_f	Flap bending stiffness
d_A, d_B	Partially deployed diagonal length
E	Young's modulus, incomplete elliptic integral of first kind
F	Tensioning or deployment force, incomplete elliptic integral of second kind
F_A, F_B	Corner forces
$f(x)$	Edge profile
H_p	Packaged height
h	Thickness
i	Strip index
k	Elliptic integral parameter
L	Side length
l	Slip
L_a, L_b	Diagonal lengths
L_c, L_f	Clip length, flap length
n	Number of strips
$\mathbf{n}$	Normal to base curve
P	Prestress per unit width
$\mathbf{p}$	Generator curve
Q_N, Q_T	Normal and tangent force components at cage exits
q	Elliptic integral, strip offset from base curve
R	Void radius
$R_{\min}$	Elastic radius of curvature
R_p	Packaged radius
$\mathbf{r}$	Base curve
s	Arclength
w	Strip width
x, y	Cartesian coordinates
δh, δv	Tip deflection components of flap
α	Involute angle
η	Packaging efficiency
θ	Involute clock angle
κ	Curvature
λ	Length normalized by h
μ	Coefficient of friction
ν	Poisson's ratio
ξ	Deployment fraction
ρ	Nondimensional deployed area
σ	Loading ratio
σ_y	Yield stress
ϕ	Thickness multiplier, elliptic integral amplitude
χ	Maximum slip normalized by h
ψ	$R_{\min}$ normalized by h

2.1. Uniaxial packaging

Well-known techniques for one-dimensional packaging include: z-folding, wrapping (or rolling), and fan-folding. These techniques provide efficient packaging, can easily accommodate the thickness of the membrane, and can avoid plastic deformation. Deployment and pretensioning can be carried out by a simple, uniaxial deployment mechanism, e.g. with a linear actuator such as a telescopic boom. Typically, a spreader bar attached to the edge of the membrane is used to hold the membrane in tension. For example, the first set of solar arrays for the Hubble Space Telescope adopted a rolling packaging scheme for the photovoltaic cells and two deployable booms for each wing of the array (Pellegrino, 1995), and a similar scheme has been recently adopted in the Roll-Out Solar Array (ROSA) (Spence et al., 2015).

However, only one dimension of the membrane is reduced in these packaging schemes, which are not applicable when both dimensions of the membrane exceed the available packaged envelope dimensions.

2.2. Biaxial packaging

Several solutions for the biaxial compaction of membranes have been proposed. There are two main categories that use either biaxial, translationally periodic crease lines, or asymmetric creases (Pellegrino, 2001); they will be described next. A third approach, which so far has been used only for thin-shell structures, uses cuts or slits; it will be described in Section 2.4.

Miura-ori (Miura, 1980), shown in Fig. 1a, is a well-known scheme for biaxially packaging a membrane. It modifies the standard map folding technique (i.e. double z-folding) by skewing one set of parallel fold lines. Both map folding and Miura-ori have been used for packaging space structures (Miura and Natori, 1985; Biddy and Svitek, 2012).

There are several techniques for wrapping a membrane around a polygonal hub using straight creases (Guest and Pellegrino, 1992; Zirbel et al., 2013), see the two examples of 6-fold symmetric crease patterns to wrap a flat membrane around a hexagonal hub, in Fig. 1(b and c). The curvature of the near-radial crease lines is related to the thickness of the membrane. The coordinates of the vertices of the crease pattern are computed such as to provide sufficient spacing between vertices that fall in the same meridional plane, in the wrapped configuration. The crease lengths and angles are computed by considering both the flat and the wrapped configurations of the membrane, but without considering any intermediate configurations.

It is also possible to compact membranes biaxially by first folding in one direction and then wrapping. Both z-folding and wrapping (Montgomery and Adams, 2008; Biddy and Svitek, 2012), and star folding and wrapping (Furuya et al., 2011) have been proposed. These approaches require the crease lines to be curved to accommodate the thickness of the membrane (Lee and Close, 2013; Lee and Pellegrino, 2014; Satou and Furuya, 2013), as is shown in Fig. 2.

2.3. Thickness effects

The effect of material thickness must be considered, especially near the fold lines and the vertices where the fold lines intersect. In the case of uniaxial packaging, this is straightforward. The hinge axes of the folds can be shifted to either the top or the bottom surface of the material, as illustrated in Fig. 3. This is known as the *axis shift* method (Edmondson et al., 2014). For biaxial packaging, the amount of axis shift for each fold line at a vertex must be determined to ensure that the vertex is not overconstrained. The amount of axis shift that allows folding has been determined for symmetric degree-4 vertices (Hoberman, 1988) and for any vertex (Chen et al., 2015). Structures with these specific hinge axis offsets have a stepped shape, as different panel thicknesses are needed to provide the appropriate axis shifts. Since the hinge axes are not coplanar in the fully deployed state, the kinematics of such structures do not follow those of an equivalent, zero-thickness origami pattern.

A variant of the axis shift approach is to allow sliding along the hinge lines (Trautz and Künstler, 2009). This enables the hinge axis offsets to have arbitrary values. However, fully folding a vertex with sliding hinges without allowing any deformation of the panels would require an infinite amount of sliding.

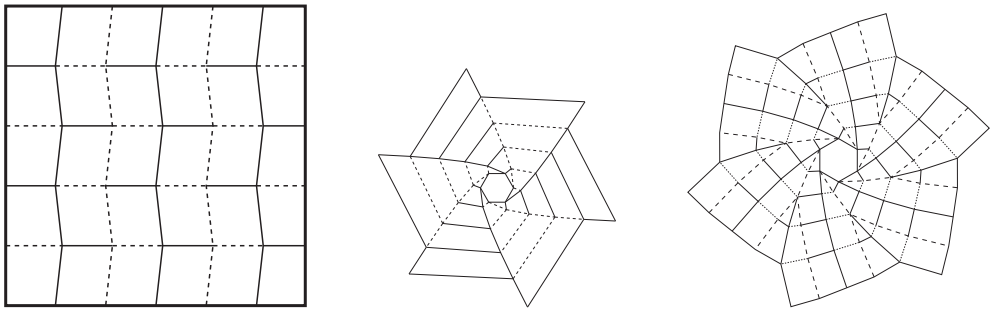

(a) Miura-ori (b) Guest & Pellegrino, 1992 (c) Zirbel et al., 2013

Fig. 1. Fold patterns for biaxial compaction of membranes. Hill folds are shown as solid lines, valley folds as dotted lines.

(a) Crease pattern (b) Model, deployed (c) Model, folded

Fig. 2. Curved crease folding. Hill folds are shown as solid lines, valley folds as dotted lines.

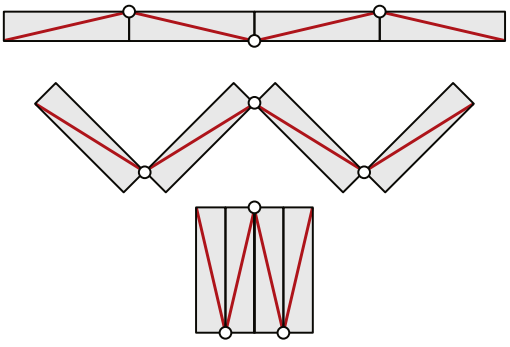

Fig. 3. Hinge axis shift method for accommodating thickness.

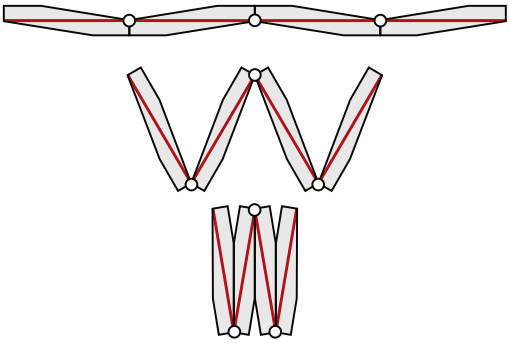

Fig. 4. Volume trimming method for accommodating thickness.

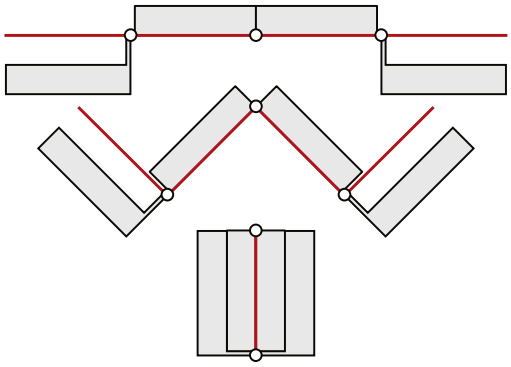

Fig. 5. Offset panel method for accommodating thickness.

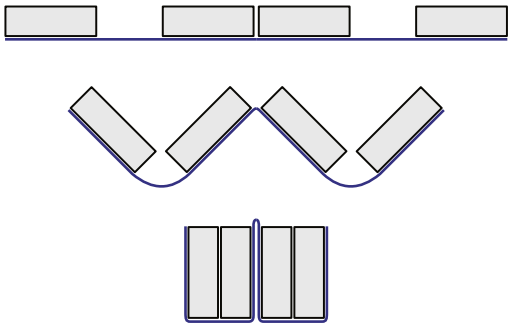

Fig. 6. Membrane with thinner strips for accommodating thickness.

An alternative method that preserves the kinematics of the underlying origami pattern, called *volume trimming* (Tachi, 2011), is shown in Fig. 4. Note that the hinge axes remain planar, and material close to the hinge axes is removed to allow folding. However, this method requires variable-thickness panels and the amount of material to be removed is a function of the final fold angle; as this angle approaches ± 180°, more and more material must be removed. In the limit of panels that rotate 180° all material must be removed.

To address these issues with the volume trimming method, it has been proposed to offset the panels from the hinge axes by means of standoffs (Edmondson et al., 2014), as shown in Fig. 5. The resulting panels have uniform thickness and can be folded fully, however the construction of the standoffs may be problematic. Additionally, the unfolded structure does not present flat, coplanar faces.

Another approach is to connect thick panels with thinner strips, leaving gaps between the thick panels where necessary (Zirbel

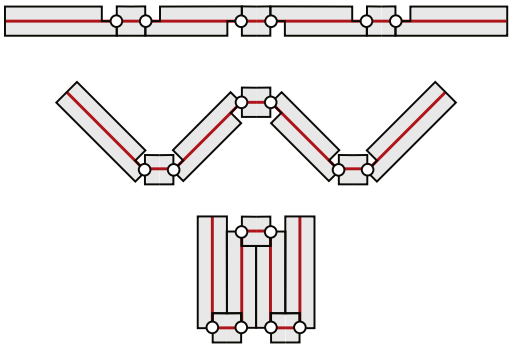

Fig. 7. Offset creases for accommodating thickness.

et al., 2013; Reynolds and Murphey, 2014), as illustrated in Fig. 6. The thinner strips introduce additional compliance in the deployed structure, which is usually undesired. A further issue is that during deployment the structure does not follow the kinematics of a flat origami.

A variant of this last approach was proposed for flat-foldable origami (Ku and Demaine, 2015), see Fig. 7. This technique replaces the compliant strip in the fold region with two separate hinges. The relationship between the kinematics of such a structure and those of its origami counterpart introduces additional complexity.

2.4. Cuts and slits

A radically different approach to packaging is to introduce a series of discontinuities, or cuts, instead of creases or hinges. This approach was first introduced to enable packaging of curved structures, and it was found that a wide range of packaging schemes could be enabled by introducing localized cuts in thin shells. Packaging schemes for thin-shell reflectors using either radial cuts (Tibbalds et al., 2004; Reynolds et al., 2011) or spiral cuts (Greschik, 1996) have been proposed but, to the authors' knowledge, this approach has not been considered for membrane packaging. It should be noted, though, that the stripped solar sail design by Greschik and Mikulas (2002) put forward an architecture that consists of separate parallel strips. Greschik and Mikulas (2002) argued that a membrane cut into strips has a statically determinate stress distribution, and hence this approach provides a more robust and reliable design than a continuous membrane.

Since cutting a membrane into strips introduces additional deformation mechanisms that also facilitate packaging, the particular approach chosen by Greschik and Mikulas is the inspiration for the approach presented in this paper.

3. Wrapping with slipping folds

Consider a square membrane of side length L and thickness h, as shown in Fig. 8. This membrane is divided into n strips by introducing $n-1$ slipping folds. A *slipping fold* allows rotation around

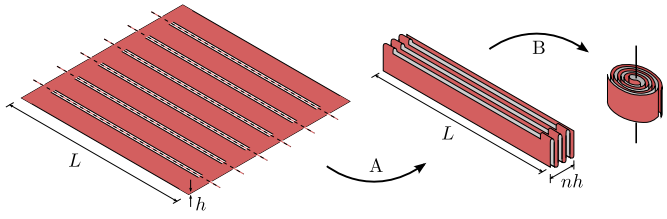

Fig. 8. Packaging concept consists of two steps: (A) z-folding and (B) symmetric wrapping.

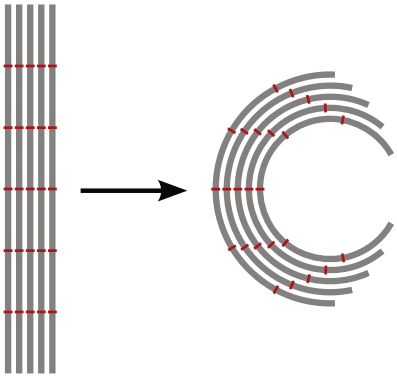

Fig. 9. Wrapping a stack of thick inextensible strips requires them to slip against each other.

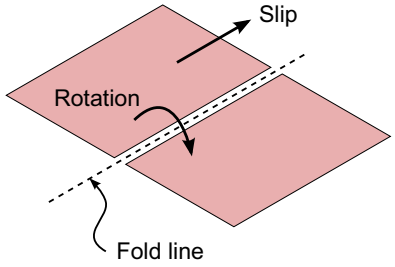

Fig. 10. Slipping folds have two degrees of freedom: rotation around the fold line and translation along the fold line.

the fold line as well as translation along the fold line. In Fig. 8 the slipping folds are shown as a series of parallel slits in the membrane, but there are many ways of realizing a slipping fold, as discussed in Section 3.1.

The packaging concept, first presented in Arya et al. (2015), involves two separate steps. First, the membrane is *z-folded* to produce a stack of n strips. Second, this stack of strips is wrapped in a *two-fold rotationally symmetric way*. Note that, during this second step, the slipping folds are needed to accommodate the incompatibility created by wrapping the membrane strips around different radii, as seen in Fig. 9. The two-fold rotationally symmetric wrapping reduces to zero the slip at the edges of the membrane, allowing the outer edge to remain continuous. The details of this packaging scheme are explained next.

3.1. Slipping folds

The proposed packaging concept relies on the existence of parallel lines of discontinuity in the membrane, along which folding and slipping can take place without any strain in the material. Placing straight cuts in the membrane is the easiest physical implementation of this concept, although several alternative implementations are possible.

The two kinematic degrees of freedom at a slipping fold are shown in Fig. 10. In addition to rotation around the fold line, the fold also allows translation along the fold line, herein termed *slip*. In practice the amount of slip required to package a given membrane can be calculated, and hence the design of the slipping folds can be targeted to providing this specific amount of slip.

The slip degree of freedom is required to enable the wrapping step in stage B of Fig. 8, because wrapping the z-folded stack of n strips requires the outer strips to go around larger radii than the inner strips. Thus, for the same arclength, the outer strips traverse smaller wrapping angles than the inner strips. If the strips cannot slip against each other, wrapping the stack of strips will result in straining or micro-buckling of the membrane.

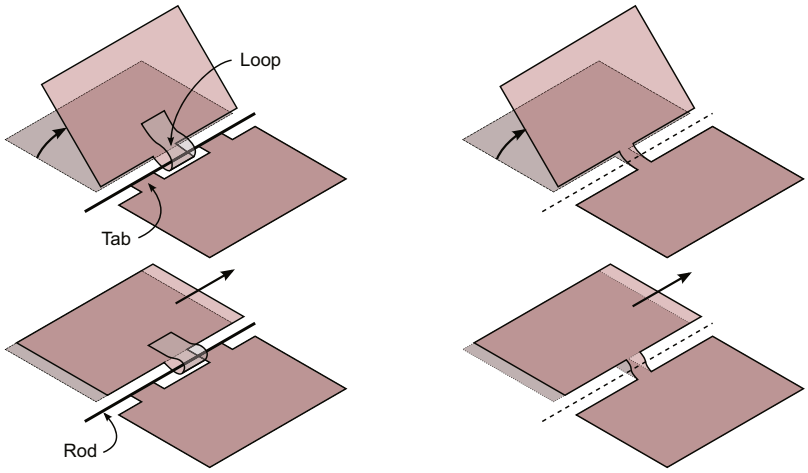

(a) Hinged fold. (b) Ligament fold.

Fig. 11. Examples of slipping folds that provide a partial connection across the fold line.

Because a full discontinuity would significantly reduce the stiffness of the membrane, several realizations of slipping folds have been considered that preserve some degree of continuity. Two concepts that allow the transmission of tension forces and of limited shearing forces across a fold line are shown in Fig. 11. The first concept is the hinged fold, Fig. 11(a), consisting of a flexible rod enclosed within loops attached to alternate sides of the membrane. The gaps between the loops define the maximum slip that is allowed and tension can be transmitted across the fold line. The concept in Fig. 11(b) is a ligament fold, consisting of a series of slender pieces of membrane that join the strips across the fold line. The length of the ligaments is chosen such as to allow for the required rotation and slip without any plastic deformation of the ligaments. Hence, like the hinged fold, the ligament fold is also designed for the required maximum slip. A ligament fold allows for the transmission of tension and a small amount of shear across the fold line. Whereas hinged folds are more suitable for larger structures where mechanical complexity may be appropriate, ligament folds are useful for small scale prototypes.

3.2. Wrapped configuration

In the packaged configuration, the mid-surface of each strip lies on a cylindrical surface, which in Fig. 8 is shown with a vertical axis. Imposing the constraint that the strips are nested, the mid-surfaces of all strips can be determined by fixing the shape of the mid-surface of a reference strip. Then, once all strips have been determined, the amount of slip between them, the maximum strain in the strips and the overall packaging efficiency can all be determined.

The problem of determining the shape of the packaged configuration is analyzed by determining the intersection between the mid-surface of each strip and the horizontal plane shown in Fig. 8. The chosen reference curve, called the *base curve*, is defined as the center line of this set of curves.

The base curve is parametrized by its arclength s,

$$\mathbf{r}(s) : [-L/2, L/2] \to \mathbb{R}^2 \tag{1}$$

As shown in Fig. 12, the strips are indexed by positive integers on one side of the base curve, and negative integers on the other. If n is odd, the index i takes integer values between $-(n-1)/2$ and $(n-1)/2$, and $i = 0$ corresponds to the central strip and the base curve. If n is even, i has integer values between $-n/2$ and $n/2$, and $i = 0$ corresponds to the base curve, but not to a strip.

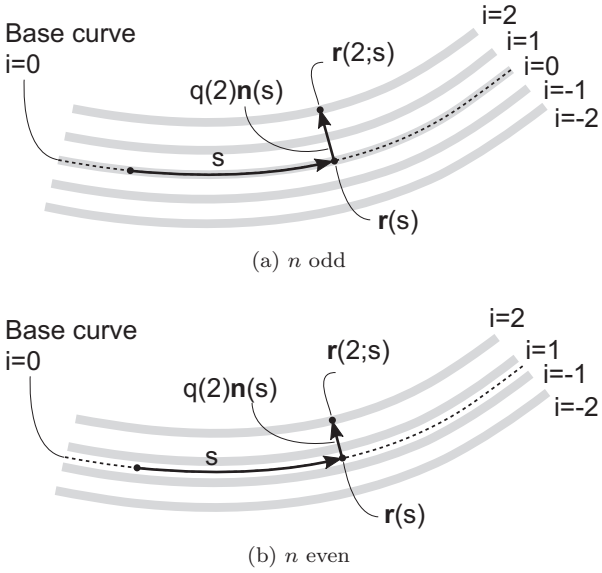

(a) n odd

(b) n even

Fig. 12. Offset curves have index i and are uniformly separated from the base curve. The base curve is represented by a dashed line.

The mid-surface of the ith strip, see Fig. 12, is offset from the base curve by $q(i)\mathbf{n}(s)$, where $\mathbf{n}(s)$ is the normal to the base curve and $q(i)$ is the separation distance. Thus, the center line of the ith strip is defined by the offset curve

$$\mathbf{r}(i; s) = \mathbf{r}(s) + q(i)\mathbf{n}(s) \tag{2}$$

where

$$q(i) = \begin{cases} i\phi h & \text{if } n \text{ is odd} \\ i\phi h - \frac{\phi h}{2}\operatorname{sgn}(i) & \text{if } n \text{ is even} \end{cases} \tag{3}$$

and ϕ is a strip thickness multiplier ($\phi \geq 1$) that accounts for the fact that in the packaged configuration the strip center lines may be separated by a distance slightly greater than the thickness of the membrane.

Once the strip center lines are known, the slip $l(i; s)$ between the $(i+1)$th and the ith strip can be expressed in terms of the arc length s of the base curve. The slip $l(i; s)$ is defined as the difference between the arc lengths s_{i+1} and s_i of the two strips:

$$l(i; s) \equiv s_{i+1}(s) - s_i(s) \tag{4}$$

The arclength of strip i has the expression

$$s_i(s) = \int_{s_0}^{s} \|\mathbf{r}'(i;\tilde{s})\|\,\mathrm{d}\tilde{s} \tag{5}$$

where s_0 is some point along the base curve where the slip is identically 0, and $\tilde{s}$ is a dummy variable of integration corresponding to the arclength s. The tangent vector $\mathbf{r}'(s)$ is obtained by differentiating Eq. (2):

$$\|\mathbf{r}'(i;s)\| = \|\mathbf{r}'(s) + q(i)\mathbf{n}'(s)\| \tag{6}$$

The derivative of the normal vector, $\mathbf{n}'(s)$, is parallel to the tangent vector and has length $|\kappa(s)|$ (Spivak, 1999), where $\kappa(s)$ is the signed curvature of the base curve:

$$\mathbf{n}'(s) = -\kappa(s)\mathbf{r}'(s) \tag{7}$$

Substituting Eq. (7) into Eq. (6) and noting that $\|\mathbf{r}'(s)\| = 1$ gives

$$\|\mathbf{r}'(i;s)\| = 1 - q(i)\kappa(s) \tag{8}$$

Substituting Eq. (8) into Eq. (5), evaluating the resulting expression for $i+1$ and i, and then substituting into Eq. (4) gives:

$$l(i;s) = [q(i) - q(i+1)]\int_{s_0}^{s} \kappa(\tilde{s})\,\mathrm{d}\tilde{s} \tag{9}$$

Finally, substituting Eq. (3) gives:

$$l(i;s) = \phi h \int_{s_0}^{s} \kappa(\tilde{s})\,\mathrm{d}\tilde{s} \tag{10}$$

Note that, according to Eq. (10), the slip between two adjacent strips is independent of the index i and hence the design of the slipping folds (e.g. the length of the ligaments) can be the same for all strips. Eq. (10) provides the relative slip between two sections, at arclengths s_0 and s of the base curve, and it is particularly useful to choose s_0 at a location where the slip is zero. The maximum slip, $l_{\max}$, is a key design parameter for slipping folds.

For example, consider the square membrane shown in Fig. 8. We choose $s_0 = -L/2$, where there is no slip between the strips because they are continuous along the edge of the square, and set $l(i; L/2) = 0$ to enforce zero slip also at the other end of the stack. Hence, we obtain:

$$\int_{-L/2}^{L/2} \kappa(s)\,\mathrm{d}s = 0 \tag{11}$$

A simple way to meet this condition is to choose $\kappa(s)$ as an odd function of the arclength, i.e. $-\kappa(-s) = \kappa(s)$. A base curve that has this property may be defined in a piecewise manner, using a *generator curve* $\mathbf{p}(s) : [0, L/2] \to \mathbb{R}^2$ and a copy of the generator curve rotated by 180°:

$$\mathbf{r}(s) = \begin{cases} -\mathbf{p}(-s) & \text{if } s \in [-L/2, 0) \\ \mathbf{p}(s) & \text{if } s \in [0, L/2] \end{cases} \tag{12}$$

Eq. (12) defines a wrapping with two-fold rotational symmetry, and hence it has been shown that a two-fold rotationally symmetric wrapping scheme is a sufficient (though not necessary) condition for having zero slip at both ends of the wrapped stack.

3.3. Simple geometric solution

A simple example of a base curve that provides compact wrapping is the piecewise curve in Fig. 13, consisting of a semi-circle of radius R, a straight line of length c, and an involute of a circle with pitch $2\pi c$. An involute of a circle is a spiral-like curve with the property that the normal distance between successive turns remains constant. This distance is the pitch of the involute, and it can be set equal to $2\phi nh$ to account for the thickness of the $2n$ strips that must fit between successive turns of the involute, as is shown in Fig. 13(b):

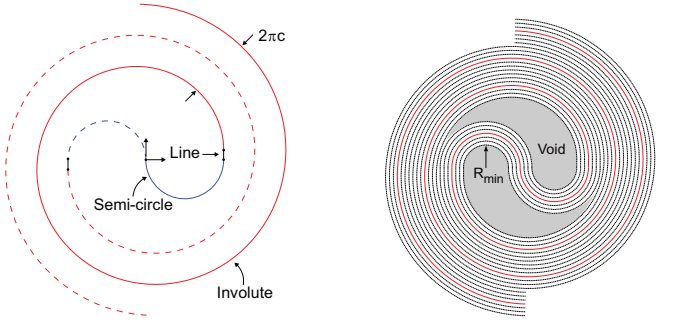

(a) Base curve (b) Offset curves

Fig. 13. Example of base curve that provides compact packaging. The shaded areas in (b) are the only voids that result from this curve, and their size depends mainly on the minimum radius of curvature $R_{\min}$.

$$\mathbf{p}(s) = \begin{cases} R\{1 - \cos(s/R), -\sin(s/R)\} & \text{if } s \in [0, \pi R] \\ R\{2, (s/R) - \pi\} & \text{if } s \in (\pi R, \pi R + c) \\ c\{\cos(\alpha - \theta) + \alpha \sin(\alpha - \theta), \\ \quad \sin(\alpha - \theta) - \alpha \cos(\alpha - \theta)\} & \text{if } s \in (\pi R + c, L/2) \end{cases} \tag{13}$$

$$\text{with:} \quad \alpha^2 = \frac{2}{c}(s - \pi R - c) + \left(\frac{2R}{c}\right)^2 \tag{14}$$

$$\theta = \frac{2R}{c} - \frac{\pi}{2} \tag{15}$$

Due to the curvature discontinuities that have been assumed in defining this simple base curve, an actual wrapped membrane will not follow this curve exactly. However, this simple, geometrically defined curve may be used to obtain preliminary, analytical estimates of maximum slip and packaging efficiency.

The radius of the semi-circle can be defined such as to avoid plastic deformation of the most tightly wound membrane strip, i.e. the strip that is curved with radius $R_{\min}$, where

$$R_{min} = R - \frac{\phi h n}{2} \tag{16}$$

Hence, given the elastic modulus, E, Poisson's ratio, ν, and yield stress, σ_y of the membrane, the Tresca yield criterion can be used to estimate the minimum radius of longitudinal curvature of an initially flat strip that is wrapped on a cylinder:

$$R_{min} \geq \frac{Eh}{2(1-\nu^2)\sigma_y} \tag{17}$$

3.4. Maximum slip

For the particular solution described in Section 3.3 the curvature $\kappa(s)$ is entirely negative for one sign of s and entirely positive for the other sign. Hence, the magnitude of l obtained from Eq. (10), grows monotonically from one end of the strip to $s = 0$, and then it decreases monotonically. Thus, it follows that $l_{\max}$ occurs at the center of the curve, at $s = 0$, and it has the following expression:

$$l_{max} = \phi h \int_{-L/2}^{0} \kappa(s)\,\mathrm{d}s = \phi h \int_{0}^{L/2} \kappa(s)\,\mathrm{d}s \tag{18}$$

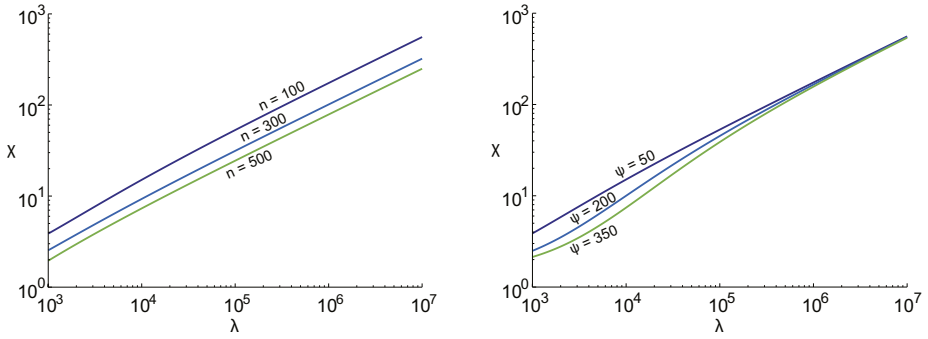

(a) $\phi = 1, \psi = 50$ (b) $\phi = 1, n = 100$

Fig. 14. Variation of non-dimensional maximum slip χ with non-dimensional membrane size λ, for $\phi = 1$; (a) for different n but constant ψ, and (b) different ψ but constant n.

where $\kappa(s)$ can be calculated from Eq. (13) by noting that $\kappa(s) = -\mathbf{r}'(s) \cdot \mathbf{n}'(s)$:

$$\kappa(s) = \begin{cases} 1/R & \text{if } s \in [0, \pi R] \\ 0 & \text{if } s \in (\pi R, \pi R + c) \\ 1/[c\alpha(s)] & \text{if } s \in (\pi R + c, L/2) \end{cases} \tag{19}$$

Integrating Eq. (19) gives:

$$\int \kappa(s)\, \mathrm{d}s = C + \begin{cases} s/R & \text{if } s \in [0, \pi R] \\ \pi & \text{if } s \in (\pi R, \pi R + c) \\ \pi - 2R/c + \alpha(s) & \text{if } s \in (\pi R + c, L/2) \end{cases} \tag{20}$$

and substituting Eq. (19) into Eq. (18) gives:

$$l_{max} = \phi h \int_0^{L/2} \kappa(s)\, \mathrm{d}s = \phi h \left(\alpha_{max} + \pi - \frac{2R}{c} \right) \tag{21}$$

Defining the non-dimensional slip:

$$\boxed{\chi \equiv \frac{l_{max}}{h}} \tag{22}$$

we obtain:

$$\chi = \phi \alpha_{max} - \frac{2\pi\psi}{n} \tag{23}$$

with

$$\alpha_{max} = \sqrt{\frac{\pi\lambda}{n\phi} + \frac{2\pi^2\psi}{n\phi} - 2 + \left(\frac{2\pi\psi}{n\phi} \right)^2} \tag{24}$$

where the non-dimensional minimum bend radius is defined as

$$\boxed{\psi = \frac{R_{min}}{h}} \tag{25}$$

and the non-dimensional strip length is defined as

$$\boxed{\lambda = \frac{L}{h}} \tag{26}$$

Fig. 14 shows plots of the variation of the non-dimensional maximum slip χ with the non-dimensional length λ for different values of n and ψ, with ϕ held constant. As λ becomes larger, the dominant term in Eq. (24) is the first term and hence, from Eq. (23), the maximum slip grows with the square-root of λ. Hence,

$$\text{for } \lambda \to \infty, \quad \alpha_{max} \to \sqrt{\frac{\pi\lambda}{n\phi}} \quad \text{and} \quad \chi \to \sqrt{\frac{\pi\phi\lambda}{n}}$$

This result implies that the proposed concept incurs a less-than-proportional increase in maximum slip when it is applied to larger membranes, while keeping constant the thickness.

3.5. Packaging efficiency

The wrapped membrane stack is contained within a cylinder of radius

$$R_p = \max \|\mathbf{r}(i; s)\| \tag{27}$$

and height

$$H_p = \frac{L}{n} \tag{28}$$

Hence, the packaging efficiency, η, is defined as the ratio between the volume enclosed by this cylinder and the volume of membrane material. It is given by

$$\boxed{\eta = \frac{L^2 h}{\pi R_p^2 H_p}} \tag{29}$$

It can be shown that the packaging efficiency is a function of four non-dimensional parameters: the number of strips n, the non-dimensional minimum bend radius ψ, the length-to-thickness ratio λ, and the thickness multiplier ϕ. It has the following expression:

$$\eta = \frac{n\lambda}{\pi\phi^2} \left[\left(\frac{n}{\pi} \right)^2 + \left(\frac{n\alpha_{max}}{\pi} \right)^2 + \left(\frac{n-1}{2} \right)^2 + \frac{n(n-1)}{\pi} \alpha_{max} \right]^{-1} \tag{30}$$

The variation of the packaging efficiency with these parameters can be better understood with the aid of Fig. 15, showing the effects of λ, ψ, and ϕ. It can be seen in Fig. 15(a) that the strip thickness multiplier ϕ has the greatest effect for large λ. In fact,

$$\text{as } \lambda \to \infty, \quad \eta \to 1/\phi \tag{31}$$

This result implies that for very large or very thin membranes, the global packaging efficiency depends mainly on the amount of empty space that is left around each strip. The plots in Fig. 15(b) show the effects of varying the minimum bend radius of the membrane, $R_{\min}$. Since from Eq. (25) $R_{\min} = h\psi$, increasing ψ, and hence increasing $R_{\min}$ causes a significant reduction in packaging efficiency for small λ. As λ increases, the size of the two voids at the center of the wrapped membrane (which is determined by $R_{\min}$), shown in Fig. 13, becomes smaller in relation to the overall membrane volume, and hence the effect of ψ decreases.

Also note that the effect of the number of strips n on the packaging efficiency is minimal since, as n increases, the height of the package decreases but also the radius increases, and thus the packaged volume varies only minimally.

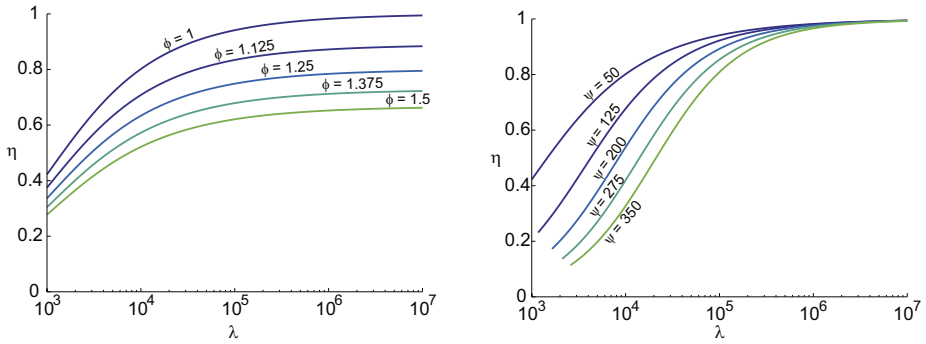

(a) $n = 100, \psi = 50$ (b) $n = 100, \phi = 1$

Fig. 15. Variation of packaging efficiency η with dimensionless deployed length λ, for $n = 100$ and (a) different values of ϕ but constant ψ and (b) different values of ψ but $\phi = 1$.

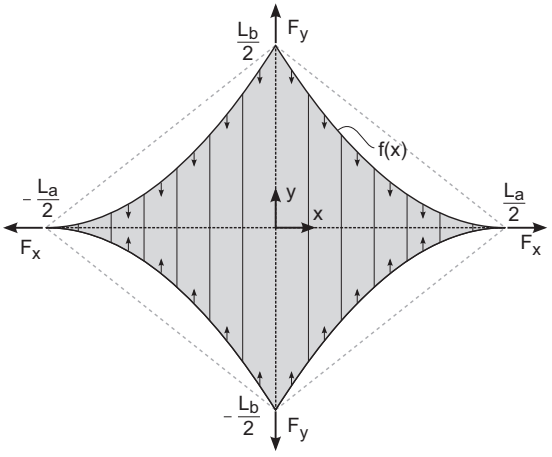

Fig. 16. Membrane with parabolic edges, loaded by corner pairs of diagonal forces, and subject to uniform uniaxial tension per unit width.

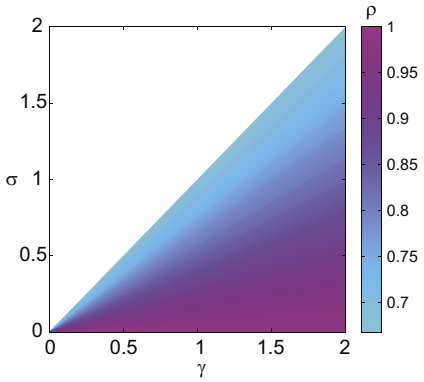

Fig. 17. Normalized membrane area as function of aspect ratio and loading ratio. The upper triangular region is inaccessible because $f'(L_a/2) \le 0$.

4. Prestressing concept

After deployment, the membrane must be pretensioned to stabilize it in the flat configuration. A further advantage of the proposed discontinuous structural architecture, chosen because of its packaging advantages, is that it is compatible with a statically determinate pretensioning scheme.

The symmetric wrapping scheme presented in Section 3 allows the edges of the membrane to remain continuous; hence, a tension force can be applied along the edge of the membrane and, by shaping the edge profile, this edge tension can be used to induce a uniform prestress in the inner part of the membrane. This approach is a continuum version of a standard approach in the design of suspension bridges (Irvine, 1981).

Consider the membrane shown in Fig. 16, with slipping folds parallel to the y-axis, and diagonal lengths L_a along the x-axis and L_b along the y-axis. It is desired that each strip has uniform pretension in the y-direction, i.e. parallel to the slipping folds, and no pretension in the x-direction, i.e. perpendicular to the slipping folds.

The desired, uniform uniaxial tension per unit width P in the membrane, acting in the y-direction, is in equilibrium with corner forces F_x at $[\pm L_a/2, 0]$ and F_y at $[0, \pm L_b/2]$ applied by suitable external compression members, e.g. deployable booms or masts, and the edge profile is

$$f(x) = \left(\frac{P}{F_x}\right)x^2 - \left(\frac{PL_a}{2F_x} + \frac{L_b}{L_a}\right)x + \frac{L_b}{2}, \quad \text{for } x \in [0, L_a/2] \tag{32}$$

as shown in Fig. 16.

The remaining edges of the membrane can be defined by reflections of $f(x)$ through the x and y axes. To ensure $f(x) \ge 0$ over $x \in [0, a/2]$, the slope at the vertex must satisfy the condition $f'(L_a/2) \le 0$, and hence

$$\frac{PL_a}{2F_x} - \frac{L_b}{L_a} \le 0 \tag{33}$$

The non-dimensional parameters that control this design are the loading ratio

$$\sigma = \frac{PL_a}{2F_x} \tag{34}$$

and the aspect ratio

$$\gamma = \frac{L_b}{L_a} \tag{35}$$

Then, the membrane area A normalized by the rhombus area, $L_aL_b/2$, is denoted by

$$\rho = \frac{2A}{L_aL_b} = 1 - \frac{1}{3}\gamma\sigma \tag{36}$$

and the corner force ratio F_y/F_x, is given by:

$$\frac{F_y}{F_x} = \sigma + \gamma \tag{37}$$

Fig. 17 shows a plot of the dimensionless area as a function of σ and γ. Obviously, $\rho \le 1$, because the deployed area cannot exceed the area of the rhombus. In fact, $\rho = 1$ requires $\sigma = 0$, i.e. the membrane is unstressed.

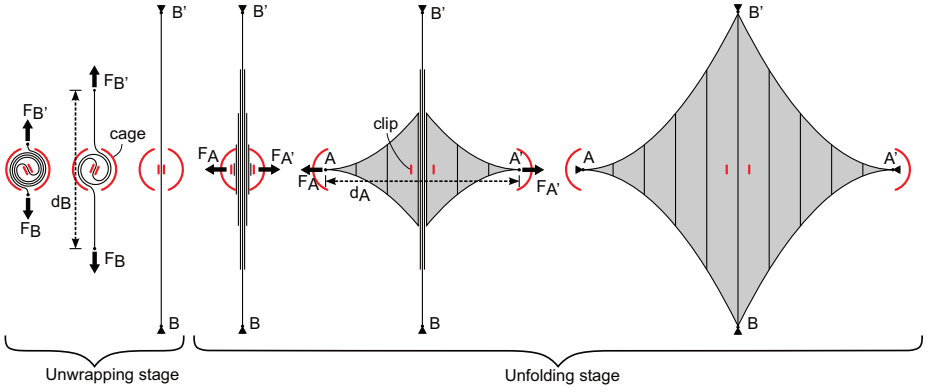

Fig. 18. Two stages of deploying a slip-wrapped membrane with parabolic edges. For clarity, only one strip is shown for the unwrapping stage.

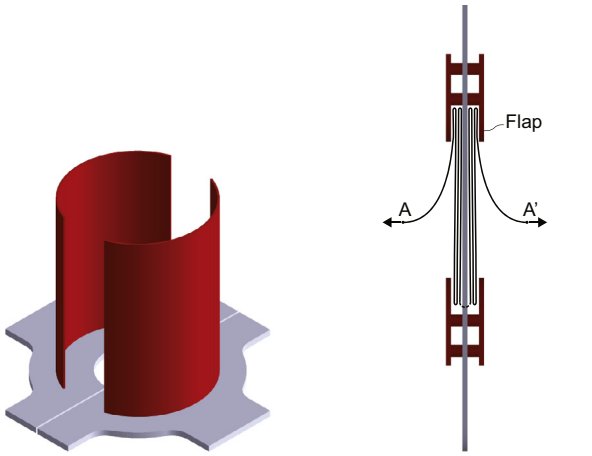

(a) Isometric view of cage (b) Clip (section view)

Fig. 19. Components of deployment restraint concept.

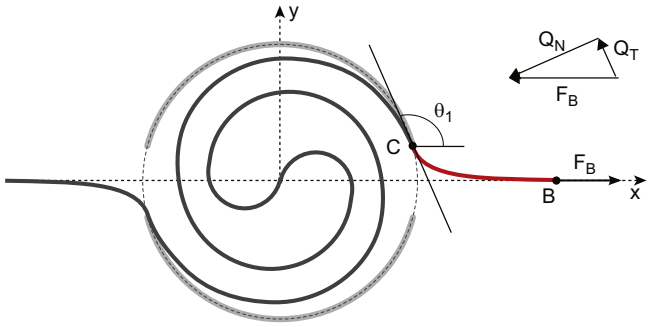

Fig. 20. Unwrapping model.

5. Deployment concept

A two-stage deployment concept for symmetrically slip-wrapped membranes with curved edges, as described in Section 4, is shown in Fig. 18. The deployment process consists of an unwrapping stage followed by an unfolding stage.

In the unwrapping stage, the two ends B and B' of the wrapped stack are pulled in opposite directions by applying forces F_B and $F_{B'}$. The separation d_B between B and B' increases until $d_B = L_b$. In the unfolding stage, the stack of strips is unfolded by applying forces F_A and $F_{A'}$ at points A and A'. The separation d_A between these points increases until $d_A = L_a$, at the end of deployment.

The deployment restraint system consists of two elements, a cage and a clip, as shown in Fig. 19. The two-part cage, Fig. 19(a), is used to control the unwrapping process. The endpoints B and B' of the packaged membrane stack are pulled out through these slots. During the unfolding stage, the two halves of the cage separate and move apart, as shown in Fig. 18. The clip, shown in Fig. 19(b), holds together the folded stack of strips, at its midpoint. It consists of four thin plates (flaps) that gradually release the strips during the unfolding stage. When the end points A and A' of the folded stack are pulled apart, the flaps bend elastically and allow a single strip at a time to deploy. Note that the wrapped membrane rotates with respect to the cage during the unwrapping stage, and hence the clip has to rotate.

5.1. Deployment forces

The first stage of the deployment process, the unwrapping of the stack, is dominated by the frictional sliding of the stack against the cage. There are also frictional interactions between the strips as they slip against each other. The wrapped stack can be modeled as an elastic rod of uniform cross-section, assuming that all strips have equal length, for simplicity, as shown in Fig. 20. It is assumed that the n strips in the stack are overlapped, and hence follow the same curve, hence the geometrical effects of strip thickness are neglected.

Each strip has modulus E, Poisson's ratio ν, width w, and thickness h, leading to a stack bending stiffness of

$$D = nE\frac{wh^3}{12(1-\nu^2)} \tag{38}$$

that is uniform over the length of the rod.

The stack is pulled at point B by a horizontal force $\mathbf{F}_B = [F_B, 0]$, parallel to the x-axis. It is assumed that no moments are applied at point B, to satisfy moment equilibrium for the free body comprising the membrane stack and the cage. The stack exits the cage at point C, where the cage applies an equal and opposite force $\mathbf{Q} = -\mathbf{F}_B$. A non-zero internal bending moment at point C ensures moment equilibrium of the arc BC, highlighted in red in Fig. 20.

At point C, the slope of the rod is denoted by θ_1 (note that the rod is not assumed to be tangent to the cage at this point), such that the normal component Q_N and the tangent component Q_T of $\mathbf{Q}$ are related through the coefficient of friction μ, hence

$$Q_T = \mu Q_N \tag{39}$$

Taking components of the forces acting at C:

$$\|\mathbf{Q}\| \sin(\pi - \theta_1) = \mu \|\mathbf{Q}\| \cos(\pi - \theta_1) \tag{40}$$

and solving for θ_1

$$\theta_1 = \pi - \tan^{-1}\left(\frac{1}{\mu}\right) \tag{41}$$

The problem of finding the profile of the unwrapping force can be posed as follows: given the location of points $B = [x_B, 0]$

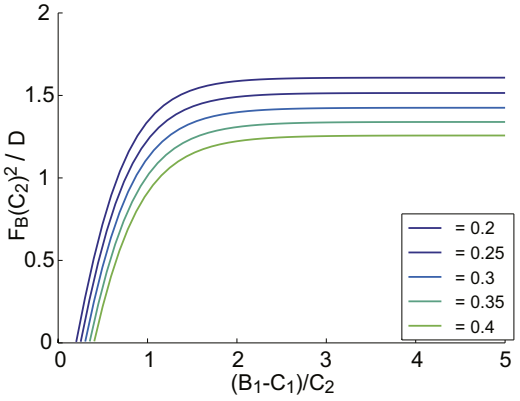

Fig. 21. Non-dimensional unwrapping force $F_B(C_2)^2/D$ with respect to non-dimensional deployment parameter $(B_1 - C_1)/C_2$.

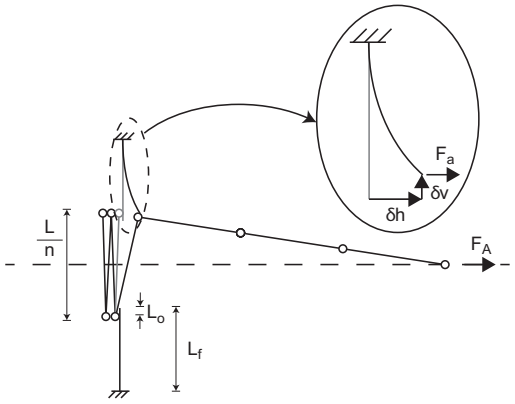

Fig. 22. Rod and hinge model to analyze deployment force F_A during unfolding process.

(determined by the imposed motion of point B) and $C = [x_C, y_C]$ (determined by the design of the slot in the cage), the bending stiffness D of the rod, find F_B such that the tangent angle is θ_1 at C and the bending moment at point B is zero. This is a standard elastica problem, whose solution is described by two coupled non-linear equations (Timoshenko and Gere, 1961):

$$y_C = \frac{2}{k} q \cos\phi_1 \tag{42}$$

$$x_B - x_C = \frac{1}{k}[F(\phi_1; q) - F(\pi/2; q)] - \frac{2}{k}[E(\phi_1; q) - E(\pi/2; q)] \tag{43}$$

Here, $F(\phi; q)$ is the incomplete elliptic integral of the first kind, and $E(\phi; q)$ is the incomplete elliptic integral of the second kind. q, ϕ_1, and k are defined as:

$$q = \sin\left(\frac{\theta_2}{2}\right) \tag{44}$$

$$\sin\phi_1 = \frac{1}{q}\sin\left(\frac{\theta_1}{2}\right) \tag{45}$$

$$k^2 = \frac{F_B}{D} \tag{46}$$

where θ_2 is the tangent angle of the rod at B.

Eqs. (42) and 43 can be solved numerically for a range of values of x_B to obtain k as a function of x_B. Then, the variation of F_B over the unwrapping process can be found using Eq. (46).

Fig. 21 plots the predictions of this model in a non-dimensional form, for various values of the coefficient of friction μ. The model predicts an initial smooth ramp up in force, followed by a plateau as the amount of total curvature in the bent stack approaches an asymptote, thus requiring less additional work. The model predicts higher values of this force plateau as the coefficient of friction decreases; this is because the tangent angle, θ_1, at point C increases with increasing coefficient of friction, μ, and at high values of θ_1, the stack needs to bend less to accommodate the boundary conditions. This model does not account for the final stages of unwrapping; when the stack is almost fully unwrapped, the contact between the stack and the cage at point C is lost, and the unwrapping force drops. The particular model described above cannot capture this behavior.

Next, we turn to the second stage of the deployment process. The deployment force F_A during the unfolding stage is mainly due to the elastic deformation of the clip; its magnitude increases as each membrane strip is pulled out and then suddenly decreases. F_A can be estimated from the simple two-dimensional model in Fig. 22, where the membrane strips are modeled as rigid rods of

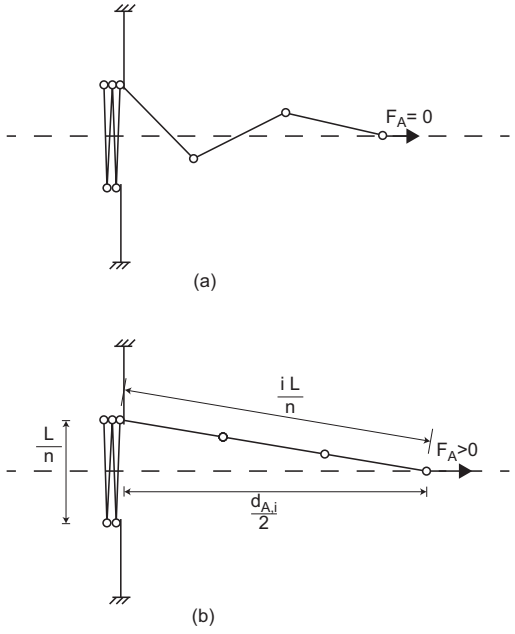

Fig. 23. Two configurations of unfolding model: (a) previously released rods are non-collinear; (b) previously released rods are collinear.

equal length connected by frictionless pin joints. The rods are held in the packaged configuration by two elastic cantilevers that represent the flaps. The thickness of the membrane is small with respect to the deployed dimensions of the membrane, and hence for simplicity it is neglected in the following analysis.

There are two different configurations of this model, depending on whether the rods that have been previously released are non-collinear, and hence $F_A = 0$, Fig. 23(a), or collinear, Fig. 23(b). In the latter case $F_A > 0$ and the next flap is deformed, until a maximum amount of deformation is reached and the hinge $i+1$ is released.

Define $d_{A,i}$ as the specific value of d_A that corresponds to the instance when F_A first becomes non-zero after the release of hinge i. This is the situation shown in Fig. 23(b). From Fig. 23(b), $d_{A,i}$ can be determined from Pythagoras' theorem:

$$\left(\frac{d_{A,i}}{2}\right)^2 + \left(\frac{L}{2n}\right)^2 = \left(\frac{iL}{n}\right)^2 \tag{47}$$

The condition for hinge $i+1$ to snap out is that the vertical deflection of the tip of the flap, δv, due to a tip of force $\sim F_A$ becomes equal to the initial overlap, L_o, between the clip and the hinge. The vertical and horizontal deflections of the flap δv and δh can be

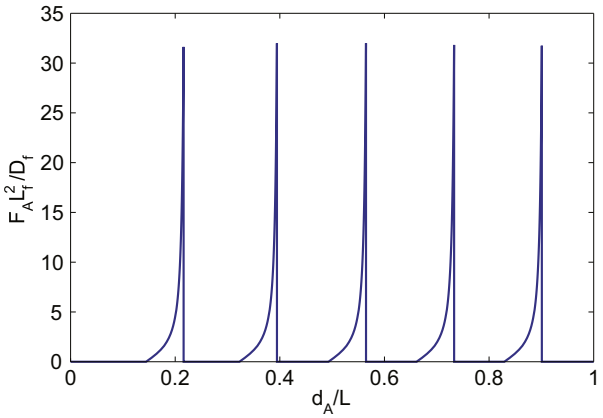

Fig. 24. Non-dimensional unfolding force $F_A L_f^2/D_f$ as a function of deployment fraction d_A/L.

calculated as a function of the applied force F_A by treating the flap as an in extensional elastic rod (Timoshenko and Gere, 1961):

$$\delta h = -\frac{2}{k}[E(\phi_1; q) - E(\pi/2; q)] - L_f \tag{48}$$

$$\delta v = \frac{2}{k} q \cos\phi_1 \tag{49}$$

Given a value of F_A, k can be calculated from:

$$k^2 = \frac{F_A}{D_f} \tag{50}$$

The deflected length of the flap is constrained to remain equal to L_f:

$$L_f = -\frac{1}{k}[F(\phi_1; q) - F(\pi/2; q)] \tag{51}$$

ϕ_1 is defined as in Eq. (45), with the value of θ_1 set to be $\pi/2$ because the flap is held vertical at the root:

$$\sin\phi_1 = \frac{1}{q}\sin\left(\frac{\theta_1}{2}\right) = \frac{1}{q}\sin\left(\frac{\pi}{4}\right) \tag{52}$$

q can be found by solving Eqs. (51) and (52). Once q has been found, δv and δh can be calculated from Eqs. (48) and (49).

This model predicts a sawtooth-like force profile: a series of smooth ramps up followed by sharp decreases in force as the flap disengages from the hinges. Fig. 24 shows the evolution of the non-dimensional unfolding force $F_A L_f^2/D_f$ with respect to the deployment fraction d_A/L for a particular choice of model parameters.

6. Experimental apparatus and test procedures

Five test models were made from aluminized polyester film, with ligament slipping folds made using a computer-controlled laser cutter (Universal Laser Systems® ILS9.75). The ligaments had widths of 1.5 mm, lengths of 8 mm, and rounded corners. Assuming $E = 3.50$ GPa and $\sigma_y = 100$ MPa for polyester films, Eq. (17) requires $R_{\min} \geq 0.89$ mm. Three models had straight edges and the remaining two had curved edges, with diagonals of equal length $L_A = L_B = L$. Further details about these models are provided in Table 1.

6.1. Packaging

A "wrapping plug" was made, to impose the required void shape in Fig. 13(b) and thus achieve the desired wrapped shape for the membrane stack. The plug also prevents the membrane from exceeding the maximum curvature limit provided by Eq. (17). The design of the plug consisted of two identical pieces, see Fig. 25, with $R_{\min} = 2$ mm, to achieve a margin of 2.25 against plastic deformation in a 50.8 μm thick polyester membrane. The two pieces were fabricated from UV-curable acrylic plastic using stereolithography. A lengthwise hole in each piece was used to assemble the plug with end plates and threaded rods. Each piece also has small pegs at either end that mate with the two end plates. These end plates hold the two halves of the plug in alignment.

To test the packaging scheme, the three models with straight edges were first folded into a stack of strips. The strips were then pre-slipped with respect to each other at the middle of the stack, before the membrane stack was inserted into the plug, by 1.1 mm, 1.7 mm, and 1.5 mm respectively for models #1, #2, and #3. This pre-slip was calculated from Eq. (21). When packaging without a plug, pre-slipping is not required since the strips are free to slip during packaging. In the present tests it was necessary to pre-slip the strips, since the plug tightly clamps the strips against each other and hence prevents slip from developing during packaging.

The strips were then tightly wrapped against the plug. A loop of string was used to hold the membrane wrapped, see Fig. 26, and a digital caliper was used to measure the diameter of the cylindrical package at mid height.

Table 1
Packaging models.

Model#	*Edges*	h (μm)	$L(m)$	λ	n	ψ
1	Straight	25.4	0.5	19,685	13	78.7
2	Straight	50.8	0.5	9842	13	39.4
3	Straight	25.4	0.9	35,433	23	78.7
4	Curved	50.8	0.8	15,748	18	39.4
5	Curved	25.4	1.0	39,370	26	78.7

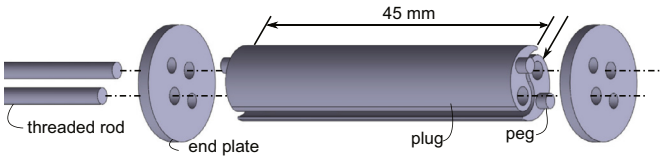

Fig. 25. Wrapping plug.

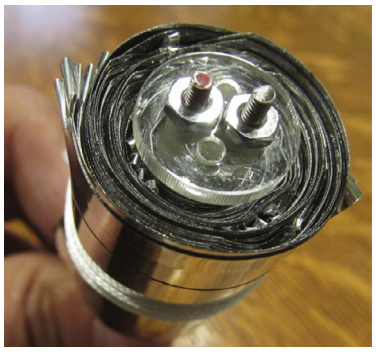

Fig. 26. Model #2 wrapped around the plug. The packaged diameter was 23.9 mm.

6.2. Prestressing

This test had the objective of demonstrating the feasibility of the prestressing concept, and was carried out on model #4. To satisfy Eq. (33) the prestress was chosen such that $\sigma = 1$; hence, Eq. (37) gives $F_y/F_x = 2$.

Fig. 27 shows the model hanging on a metal-backed chalkboard using magnets. The tensioning forces were applied by

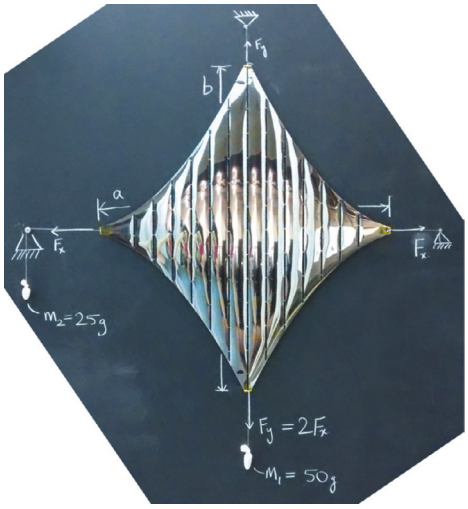

Fig. 27. Hanging model test of prestressing concept.

hanging weights: F_y was applied by hanging a 50 gm weight from the bottom corner and holding the top corner of the membrane with a pin and F_x was applied through a pulley by hanging a 25 gm weight and pinning the right corner of the membrane.

Inspection of this model showed that each strip was in a state of tension, and that the model was hanging flat. Some residual transverse curvature of the strips was observed, due to the film having been stored on a roll.

6.3. Deployment

The deployment test apparatus shown in Fig. 28 was used to test the deployment concept on model #5. The apparatus consisted of: four independent linear actuators to provide the deployment forces $F_B, F_{B'}, F_A, F_{A'}$; four force sensors to measure these deployment forces; and a suspension system to partially offload the mass of the membrane.

Each linear actuator consisted of a lead screw (with a pitch of 2.54 mm) coupled to a stepper motor that drives a carriage back and forth along a rail. Each stepper motor (1.8° full step size) was driven by a microstepping driver (Allegro™4988 driving the motor with 1/4 steps). A microcontroller (Arduino Leonardo based on an Atmel® ATmega32u4) synchronized the four motors, as well as providing logic, displacement data logging, and an interface to a laptop personal computer. One 1/4 step (corresponding to a motion of 0.003175 mm) was applied every 500 µs; slight microcontroller delays led to a carriage speed of 5.93 mm/s. The motion of each carriage was controlled in open-loop, based on the number of steps commanded.

A six-axis force sensor (ATI Industrial Automation Nano17) was mounted on each carriage, to measure the components of the deployment force with a resolution of 3.1 µN. Moment components were also measured by the sensor, but these measurements were not utilized.

Fig. 29 shows the cage, with inner diameter of 37 mm and height of 49 mm, and the clip that were used for the deployment tests. The cage consisted of two laser-cut acrylic base plates, two 125 µm-thick polyimide plates elastically bent into semicylinders by means of threaded rods that also attached the semicylinders to the base plates. The cage was constructed in two halves, which separate during the unfolding stage of the deployment. The inner faces of the semicylinders were coated with a spray-on PTFE-based dry lubricant (Saint-Gobain Fluoroglide®) to reduce friction between the cage and the membrane during unwrapping. The location of the edge of the cage in relation to its center was measured to be $x_c = 19.6$ mm, $y_c = 4.0$ mm. Note that the wrapping plugs were omitted in this test.

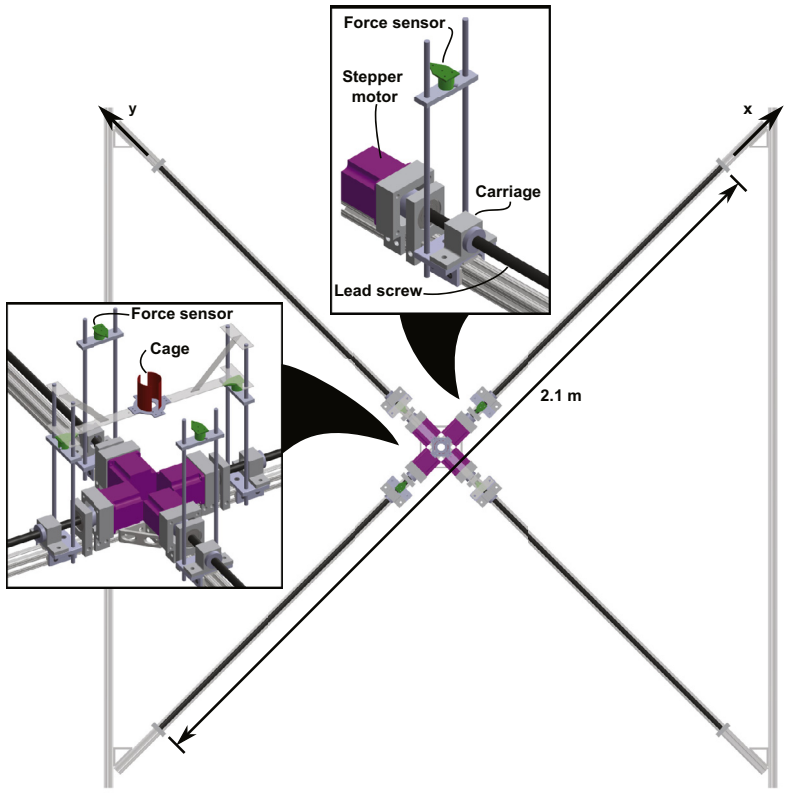

Fig. 28. Two-axis deployment rig.

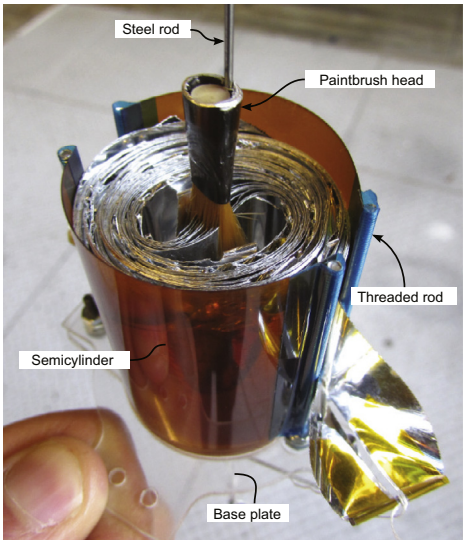

Fig. 29. Membrane model, wrapped and inserted into the cage. The cage had a diameter of 37 mm and a height of 49 mm.

The clip was made from two paintbrush heads (7 mm × 4 mm cross section, 11 mm length) connected by a steel rod. The paintbrush bristles were pushed into the wrapped membrane stack, introducing a small spacing between the membrane strips. This ensured that the membrane strips would deploy one by one.

The membrane was deployed horizontally, minimizing the effects of gravity by suspending the clip about 0.25 m above the base of the two-axis deployment rig. Since the clip holds the middle of the membrane during most of the deployment, suspending the clip helped offload some of the weight of the membrane. A 400 gm weight was suspended from the bottom of the clip to stabilize its orientation. The membrane weight was also partially offloaded at the attachment to the force sensors.

The deployment was displacement controlled at a rate of about 11.9 mm/s, by moving opposite carriages at 5.93 mm/s. Full deployment was achieved in about 4 min.

7. Test results

7.1. Packaging tests

Models #1, #2, and #3, see Table 1, were packaged according to the procedure described in Section 6.1. The packaged models had an approximately cylindrical form. The diameters of the packaged models were measured at mid-height along the axis of the cylinder, i.e., away from the ligaments and close to the restraining string. The height of each model was taken to be equal to the strip width, thus neglecting any small shift, along the axis of the cylinder, of the strips due to uneven folding. Using this measured diameter and assumed height of the cylindrical wrapped configuration of the model, the packaged volume was calculated. The material volume was taken as L^2h. From these two values, the packaging efficiencies of the models were calculated. The resulting values are plotted in Fig. 30 with respect to the length-to-thickness ratio.

Also plotted in Fig. 30 are three curves with the same n and ψ values as the three models. For each test the particular value of ϕ for which the curve passes through the experimental point was calculated and the corresponding curve has been plotted. These lines represent packaging efficiencies achievable using similar manufacturing and packaging techniques to those used in the present study, but scaled to different values of λ.

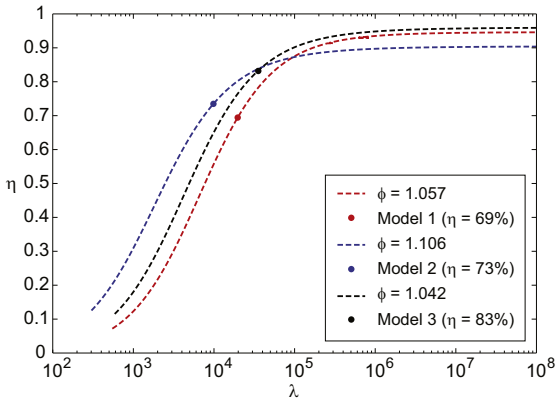

Fig. 30. Packaging test results.

Since the experimental models had been wrapped tightly and without gaps, a thickness multiplier $\phi \sim 1$ was expected. Two of the experimentally obtained values of $\phi = 1.057, 1.042$, corresponding to residual voids of around 5%, confirmed this expectation. The third measurement, with $\phi = 1.106$ and hence voids of around 11%, was obtained from the thicker model ($h = 55$ μm), which indicates that packaging with small gaps is more difficult to achieve for thicker and hence stiffer models.

7.2. Deployment tests

First, it should be noted that both during unwrapping and unfolding, the pair of forces pulling on the structure are coupled. For example, unwrapping and unfolding could be still successfully carried out if one of the two forces is set to zero as the other forces is sufficient to successfully carry out the deployment. Therefore, in comparing experimental measurements to predictions from the analytical model, it is better to focus on the mean value of the two forces.

The average deployment forces, $(F_B + F_{B'})/2$ and $(F_A + F_{A'})/2$, measured during a single deployment of model #5 are plotted in Fig. 31 with respect to the unwrapping fraction d_B/L_b and the unfolding fraction d_A/L_a. Note that the radial component of the deployment forces is dominant: the in-plane transverse deployment forces were about 20 times smaller than the radial force component, and the out-of-plane deployment forces were about 3–4 times smaller than the radial forces.

Fig. 32 shows plots of the radial component of the average deployment forces measured during three separate deployments of model #5, along with the predicted deployment forces, computed using the analytical prediction models presented in Section 5.1.

For the unwrapping force prediction, the elastic modulus was chosen as $E = 3.5$ GPa, the Poisson's ratio was $\nu = 0.38$, and the coefficient of friction was $\mu = 0.25$. The elastic properties were obtained from the manufacturer's datasheet. The coefficient of kinetic friction between an aluminized Mylar® film (the model material) and a Kapton® film treated with PTFE-based dry lubricant (the material of the cage walls) was measured in a separate experiment, in which a disc of aluminized Mylar®, glued to a known mass, was dragged over a PTFE-treated flat Kapton® sample. This was done using one of the linear actuators described in Section 6.3, and the dragging force was measured by one of the force sensors also described in Section 6.3. The coefficient of kinetic friction was extracted from the force measurements and the known mass.

For the unfolding force predictions a clip length $L_c = 11$ mm and a clip overlap $L_o = 8$ mm were used. Also, in generating the predicted unfolding force profile, a different flap bending stiffness D_f was used for each snap, to account for the increasing number

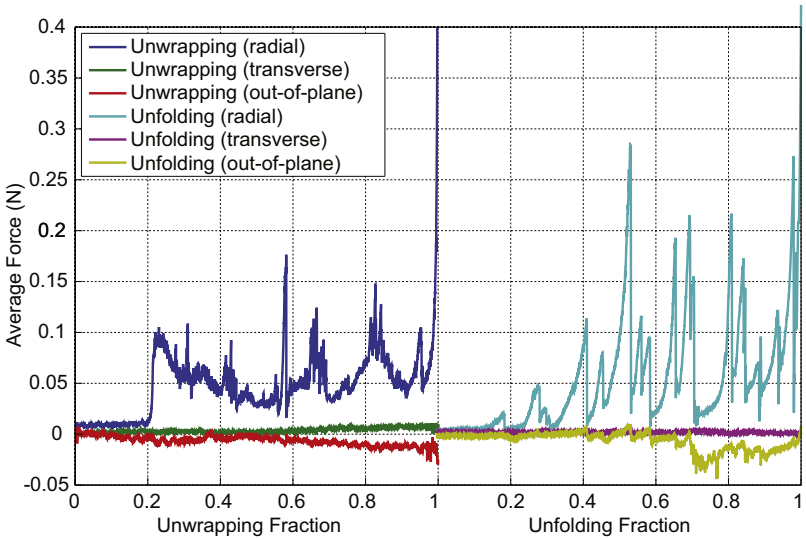

Fig. 31. Components of mean deployment forces during a single deployment of model #5. During unwrapping, the unfolding fraction is fixed at 0; during unfolding, the unwrapping fraction is fixed at 1.

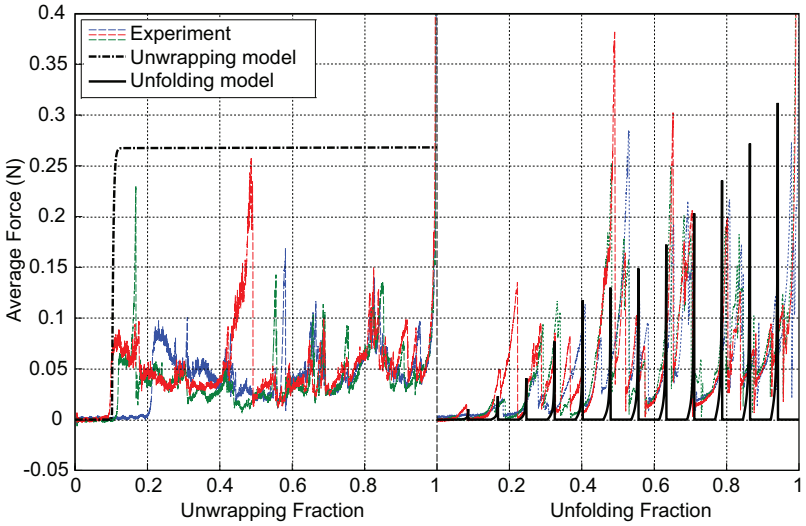

Fig. 32. Experimentally measured radial component of mean deployment forces for three separate deployments of model #5. Analytical predictions of the deployment forces are also plotted.

of paintbrush bristles engaged with the fold, which increased with successive snaps.

Regarding the comparison of experiments and predictions, in Fig. 32, it can be noted that both sets of force predictions capture the overall trends in the experimentally measured forces and their magnitude variation. Overall, there is a good match between predictions and experiments, suggesting that the physical mechanisms underlying these models (that is, friction and stack bending for the unwrapping stage and clip bending for the unfolding stage) were indeed dominant during the deployment experiments.

There are many physical effects not captured by the simple mechanical models presented in Section 5.1. These effects include gravity, contact and sliding between the strips, the non-uniform bending stiffness of the folded stack, the snagging of the folded ligaments against each other or the cage walls, and variations in the elastic and geometric properties of the crude clips. It is expected that these unmodeled effects account for most of the discrepancies between the predicted and measured deployment forces.

Fig. 33 shows photos taken by an overhead camera at the beginning of deployment, at the end of the unwrapping stage, during the unfolding stage, and at the end of the deployment.

8. Discussion and conclusion

A novel packaging scheme for thin membranes of finite thickness has been proposed. This scheme divides the membrane into parallel strips connected by slipping folds, and uses specially chosen base curves for the wrapping profile in order to avoid slippage along the outer edges of the membrane. It has been shown that a highly efficient packaging can be achieved, and also that continuity of the membrane along the edges can be maintained.

In the packaged configuration, the membrane strips are preslipped by specific amounts and are then bent smoothly around the chosen wrapping profile. This approach ensures that localized bending deformation occurs only in the ligaments between the strips, if this is the type of slipping fold that is chosen. Since localized creasing of the membrane is avoided, there is no plastic deformation and hence, after deployment, the membrane can recover its initial shape.

A scheme to apply uniform uniaxial prestress to the deployed membrane has also been proposed. This prestressing concept exploits the edge continuity of the membrane to create a catenary-like boundary that equilibrates the internal pretension. This

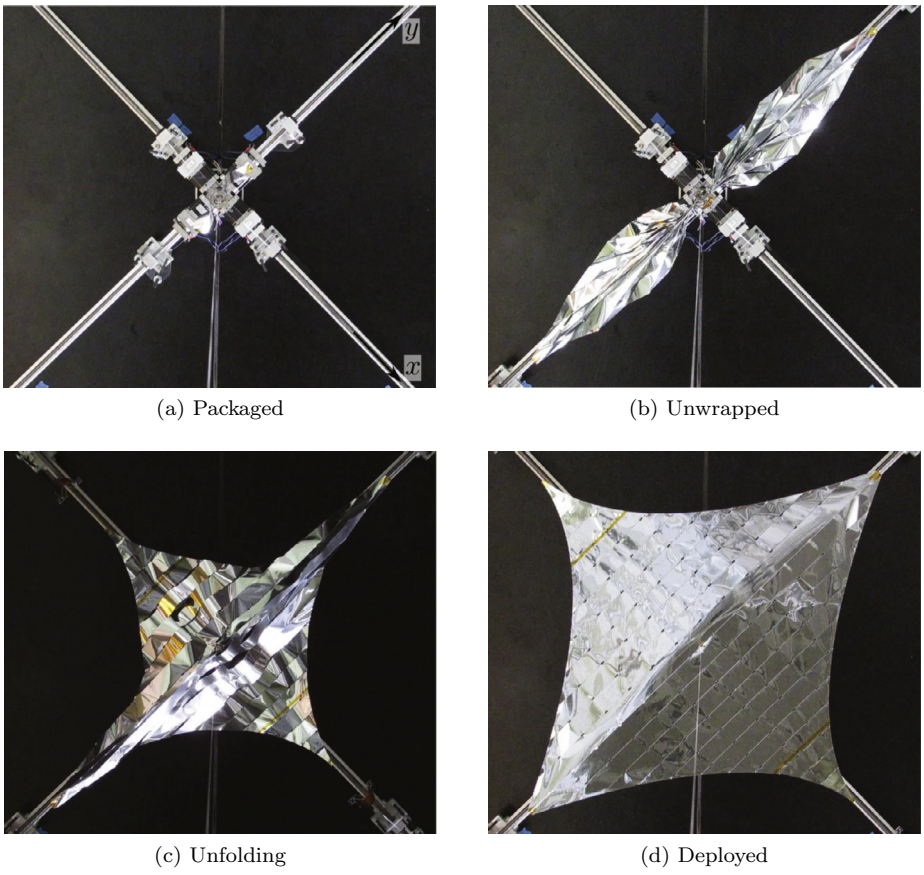

(a) Packaged (b) Unwrapped

(c) Unfolding (d) Deployed

Fig. 33. Deployment of model #5 viewed from an overhead camera.

approach requires curved membrane edges which, depending on the required level of pretension, results in a reduction in the available surface area of the membrane.

A two-stage deployment process, in which the stacked membrane strips are first unwrapped and then unfolded, has also been proposed, analyzed in detail, and demonstrated experimentally. It has been shown that the deployment is well controlled and that the corner forces required to deploy the membrane can be estimated analytically with good accuracy.

For membranes with high length-to-thickness ratios, the packaging efficiency of this concept approaches 100%. Packaging tests on meter-scale models were conducted, and packaging efficiencies of up to 83% were demonstrated at this scale.

Acknowledgments

Financial support from the Northrop Grumman Corporation is gratefully acknowledged. N. Lee was supported by a postdoctoral fellowship from the W. M. Keck Institute for Space Studies.

References

Arya, M., 2016. Packaging and Deployment of Large Planar Spacecraft Structures. California Institute of Technology Dissertation (ph.d.). doi:10.7907/Z9Z60M0D.
Arya, M., Lee, N., Pellegrino, S., 2015. Wrapping thick membranes with slipping folds. SciTech 2015, AIAA-2015-0682.
Biddy, C., Svitek, T., 2012. Lightsail-1 solar sail design and qualification. In: 41st Aerospace Mechanisms Symposium, pp. 451–463.
Chen, Y., Peng, R., You, Z., 2015. Origami of thick panels. Science 349, 6246.
Edmondson, B.J., Lang, R.J., Magleby, S.P., Howell, L.L., 2014. An offset panel technique for thick rigidly foldable origami. In: Proceedings of the ASME 2014 International Design Engineering Technical Conferences.
Furuya, H., Mori, O., Okuizumi, N., Shirasawa, Y., Natori, M.C., Miyazaki, Y., Matunaga, S., 2011. Manufacturing and folding of solar sail "IKAROS". In: 52nd AIAA/ASME/ASCE/AHS/ASC Structures, Structural Dynamics, and Materials Conference, Apr.
Greschik, G., 1996. Deployment of dishes with surface discontinuities. J. Spacecraft Rockets 33 (4).
Greschik, G., Mikulas, M.M., 2002. Design study of a square solar sail architecture. J. Spacecraft Rockets 39 (5).
Guest, S.D., Pellegrino, S., 1992. Inextensional wrapping of flat membranes. First Int. Seminar Struct. Morphol. Sept. 203–215.
Hoberman, C., 1988. Reversibly expandable three-dimensional structure. United States Patent No. 4,780,344.
Irvine, H.M., 1981. Cable Structures. MIT Press, Cambridge, Massachusetts.
Ku, J.S., Demaine, E.D., 2015. Folding flat crease patterns with thick materials. J. Mech. Robot.
Lee, N., Close, S., 2013. Curved pleat folding for smooth wrapping. Proc. R. Soc. A 469 (2155).
Lee, N., Pellegrino, S., 2014. Multi-layer membrane structures with curved creases for smooth packaging and deployment. In: AIAA SciTech Spacecraft Structures Conference, Jan.
Miura, K., 1980. Method of packaging and deployment of large membranes in space. In: Proceedings of the 31st Congress of the International Astronautical Federation IAF-80-A 31 Tokyo, pp. 1–10.
Miura, K., Natori, 1985. 2D array experiment on board a space flyer unit. Sp. Solar Power Rev. 5, 345–356.
Montgomery, E.E., Adams, C.L., 2008. Nanosail-d. CubeSat Developer's Workshop.
Murphey, T. W., 2000. A nonlinear elastic constitutive model for wrinkled thin films, Ph.D. thesis.
Papa, A., Pellegrino, S., 2008. Systematically creased thin-film membrane structures. J. Spacecraft Rockets 45 (1), 10–18.
Pellegrino, S., 1995. Large retractable appendages in spacecraft. J. Spacecraft Rockets 32 (6), 1006–1014.
Pellegrino, S. (Ed.), 2001, Deployable Structures. Springer Verlag, Wien-New York.
Reynolds, W.D., Murphey, T.W., 2014. Elastic spiral folding for flat membrane apertures. In: 55th AIAA/ASME/ASCE/AHS/ASC Structures, Structural Dynamics, and Materials Conference, Jan.
Reynolds, W.D., Murphey, T.W., Banik, J.A., 2011. Highly compact wrapped-gore deployable reflector. In: 52nd AIAA/ASME/ASCE/AHS/ASC Structures, Structural Dynamics, and Materials Conference, Apr.

Satou, Y., Furuya, H., 2013. Fold line based on mechanical properties of crease in wrapping fold membrane. In: 54th AIAA/ASME/ASCE/AHS/ASC Structures, Structural Dynamics, and Materials Conference, Apr.

Spence, B.R., White, S.F., Douglas, M.V., 2015. Elastically deployable panel structure solar arrays. U.S. Patent No. 9,156,568. 13 Oct.

Spivak, M., 1999. A comprehensive introduction to differential geometry, II, 3rd ed.

Tachi, T., 2011. Rigid-foldable thick origami. In: Yim, M. (Ed.), Origami 5, pp. 253–263.

Tibbalds, B., Guest, S.D., Pellegrino, S., 2004. Inextensional packaging of thin shell slit reflectors. Technische Mechanik 24 (3–4), 211–220.

Timoshenko, S.P., Gere, J.M., 1961. Theory of Elastic Stability, 2nd ed.. McGraw-Hill, New York, pp. 76–81.

Trautz, M., Künstler, A., 2009. Deployable folded plate structures – folding patterns based on 4-fold-mechanism using stiff plates. In: Proceedings of the International Association for Shell and Spatial Structures Symposium, Oct., pp. 2306–2317.

Zirbel, S.A., Lang, R.J., Thomson, M.W., Sigel, D.A., Walkemeyer, P.E., Trease, B.P., Magleby, S.P., Howell, L.L., 2013. Accommodating thickness in origami-based deployable arrays. J. Mech. Des. 135, 111005.